Experimental study on the Stokes effect in disordered birefringent microstructure fibers*

Zhao Yuan-Yuan(赵原源)[a)b)], Zhou Gui-Yao(周桂耀)[c)†], Li Jian-She(李建设)[b)], Zhang Zhi-Yuan(张志远)[d)], and Han Ying(韩 颖)[a)]

[a)] College of Information Science and Engineering, Yanshan University, Qinhuangdao 066004, China
[b)] College of Science, Yanshan University, Qinhuangdao 066004, China
[c)] Key Laboratory of Metastable Material Science and Technology, Yanshan University, Qinhuangdao 066004, China
[d)] College of Science, Air Force Engineering University, Xi'an 710051, China

(Received 26 December 2013; revised manuscript received 21 April 2014; published online 20 June 2014)

In this paper, a 120-fs pulse transmission experiment is carried out using disordered birefringent microstructure fibers with cladding ventages. Through this experiment, it is found for the first time that remarkable Stokes and anti-Stokes waves can also be produced when the central wavelength of the incident pulse is in the normal dispersion regime of the microstructure fiber. The generation of the two waves can be explained by the four-wave mixing phase matching theory. Properties of the two waves under the action of femtosecond laser pulses with different parameters are studied. The results show that the central wavelength of anti-Stokes waves and Stokes waves produced under the two orthogonal polarization states shift by 63 nm and 160 nm, respectively. The strengths and central positions of the two waves in birefringent fibers can be controlled by adjusting the phase match condition and the polarization directions of incident pulses.

Keywords: microstructure fiber, four-wave mixing, anti-Stokes wave, Stokes wave

PACS: 42.65.−k, 42.65.Ky, 42.70.Mp **DOI:** 10.1088/1674-1056/23/8/084208

1. Introduction

Compared with conventional fibers, microstructure fiber has many superior features, especially the excellent nonlinear and birefringent effects. The optical fields can be highly confined to a fiber core by enlarging the aperture of cladding ventages of the microstructure fiber and reducing the size of the fiber core simultaneously. This strongly confined optical field will significantly intensify the nonlinear effect. Meanwhile, the cladding structure can be designed so that the zero-dispersion points are moved to different optical bands and the central wavelength of the femtosecond laser lies in different zero-dispersion regimes of the fiber. In this way, the ultrashort pulse will produce different nonlinear effects during its transmission in the fiber, such as self-phase modulation (SPM), cross-phase modulation (XPM), four-waves mixing (FWM), and stimulated Raman scattering (SRS). The research on frequency conversion and optical soliton effects focusing on four-wave mixing has become one of the hot points of research in the current optics domain. Liu *et al.*[1] proposed the theoretical model of a nonlinear equation which governs arbitrary pump waves when the frequency intervals between pump waves are equal, and they also proved experimentally the feasibility and stability of the produced multiple four-wave mixing waves in highly nonlinear microstructure fiber with multi-frequency pump waves. Hu and Wang[2] studied the production of a super-continuum spectrum in birefringent microstructure fiber, as well as the remarkable anti-Stokes line. Comparing their model with the traditional mode coupling theory of the four-wave mixing process, Liu[3] came up with a coupled mode equation of complex amplitudes for the four waves, and studied the self-stability of the multiple four-wave mixing process in fiber both theoretically and experimentally. Most of these previous researches are focused on the stability of the multiple four-wave mixing process and the conversion efficiency of the anti-Stokes. In this paper, the influences of various parameters on the four-wave mixing with disordered cladding ventage birefringent microstructure fibers are investigated experimentally. That is, by adjusting the central wavelength, the average power of the pumping pulse, the angle between the polarization direction of pulses and the fiber short axis, the energies are converted into those of short waves and long waves efficiently. Such an efficient anti-Stokes conversion based on four-wave mixing can be widely used in wavelength conversion technology of wavelength division multiplexing (WDM), high-resolution imaging of shortwave radiation, electron transition of directly stimulated molecules, multi-photon ionization,[4–9] etc.

2. Theory and numerical simulation of the fiber properties

The photons of incident optical waves are scattered by molecules and converted into low-frequency photons; meanwhile, the molecules end their process of the transition be-

*Project supported by the National Basic Research Program, China (Grant No. 2010CB327604), the National Natural Science Foundation of China (Grant Nos. 60637010, 61205084, and 61377100), and the Science and Technology Research and Development Program of Qinhuangdao City, China (Grant No. 201101A117).

†Corresponding author. E-mail: zguiyao@163.com

© 2014 Chinese Physical Society and IOP Publishing Ltd

tween two resonance states. The incident light, as a pumping source, produces Stokes light with red-shifted frequencies. When the produced Stokes light is strong enough, it will act as a new pumping source to produce secondary Stokes and anti-Stokes waves; when the phase mismatches, i.e., $\Delta\delta = 0$, there will be remarkable four-wave mixing between pumping waves and Stokes waves, secondary Stokes waves and anti-Stokes waves. Then the parametric gain corresponds to the peak of four-wave mixing and $\Delta\delta$ can be expressed as[10,11]

$$\begin{aligned}\Delta\delta_{\mathrm{PA}} &= \beta(\omega_{\mathrm{P}}) - \beta(\omega_{\mathrm{AS}}) \\ &= (1-f_{\mathrm{R}})\gamma(\omega_{\mathrm{P}})P_{\mathrm{P}} - \sum_{n\geq 2}\frac{(\omega_{\mathrm{AS}}-\omega_{\mathrm{P}})^n}{n!}\beta_n(\omega_{\mathrm{P}}) \\ &= 0, \end{aligned} \tag{1}$$

$$\begin{aligned}\Delta\delta_{\mathrm{PS}} &= \beta(\omega_{\mathrm{P}}) - \beta(\omega_{\mathrm{S}}) \\ &= (1-f_{\mathrm{R}})\gamma(\omega_{\mathrm{P}})P_{\mathrm{P}} + \sum_{k\geq 2}\frac{(\omega_{\mathrm{S}}-\omega_{\mathrm{P}})^{2k}}{2k!}\beta_{2k}(\omega_{\mathrm{P}}) \\ &= 0. \end{aligned} \tag{2}$$

In Eqs. (1) and (2), $\beta(\omega_{\mathrm{P}})$, $\beta(\omega_{\mathrm{AS}})$, and $\beta(\omega_{\mathrm{S}})$, respectively, denote the propagation constants of the pumping wave, anti-Stokes wave, and Stokes wave, $\gamma(\omega_{\mathrm{P}})$ denotes the nonlinear coefficient, f_{R} the Roman-delayed response of quartz fibers, P_{p} the peak power of the pulse, and the corresponding angular frequency for $\Delta\delta_{\mathrm{PA}} = \Delta\delta_{\mathrm{PS}} = 0$ is just the angular frequency of the anti-Stokes wave and Stokes wave. This means that with the increase of the central wavelength of the pumping pulse, the frequency spectrum gradually broadens and the frequency shift increases. The sectional view of the fiber used in the experiment is shown in Fig. 1, in which the dark black hole represents the cladding air hole. The non-uniformity of air holes mainly brings a certain influence on the fiber birefringence, thus affecting nonlinear effects of light pulses with different incident angles. Secondly, the disordered arrangement of cladding ventages and the ellipse structure of the fiber core also allow the fiber to have a larger birefringent effect, where axes X and Y refer to the fast axis and slow axis of the fiber, respectively. In this article, we simulate basic parameters of the fiber using the finite-element method. The finite-element method has the advantage of being able to solve the microstructure fiber with arbitrary shape, size, and air hole distribution. The finite-element solution is actually the projection of a weak-form solution of differential equations in a finite dimensional space. For the partial differential equations, such as the wave equation, the finite-element method divides the closed fields expressed by the continuous function into small regions, each of which is replaced by an approximate function. Thus, the function of the whole field is discretized, resulting in a group of similar algebraic equations and the numerical approximation functions in the field through simultaneous solution. Generally, for two-dimensional (2D) problems, these regions are triangular. Triangles have larger mosaic degrees of freedom, so the field division is convenient, especially for irregular-shape boundaries. Therefore, this method has great advantages in solving microstructure fibers with irregular air holes. Figure 2 shows the model of the irregular microstructure with triangle partitions. Figure 3(a) shows the difference in propagation constant between the two orthogonal polarization modes and its functional relationship with wavelength. It can be found that the difference between propagation constants in the whole band considered is negative, which means that the X axis is the fast axis and the Y axis is the slow axis. Figure 3(b) shows the variations of birefringence and nonlinear coefficient with wavelength. The birefringence of the fiber reaches 1.3×10^{-5} at $\lambda = 800$ nm. Since the nonlinear coefficient difference between the two polarization modes is very small, Figure 3(b) only shows the nonlinear coefficient of the polarization mode of the X axis. Figure 3(c) shows the relationship between the dispersion coefficient and wavelengths of the two orthogonal polarization modes. Zero-dispersion points of X and Y polarization modes are at wavelengths of 993 nm and 997 nm, respectively.

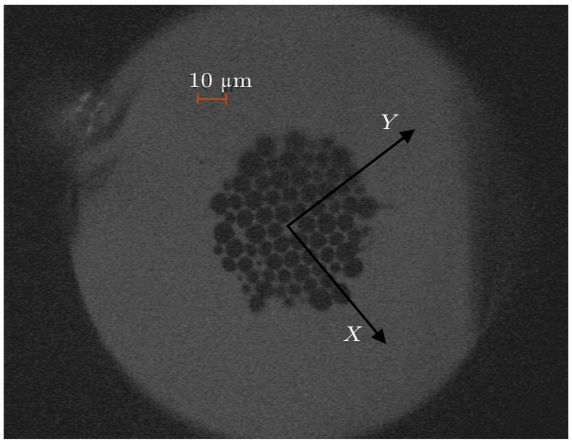


Fig. 1. Cross section of the PCF used in the experiment.

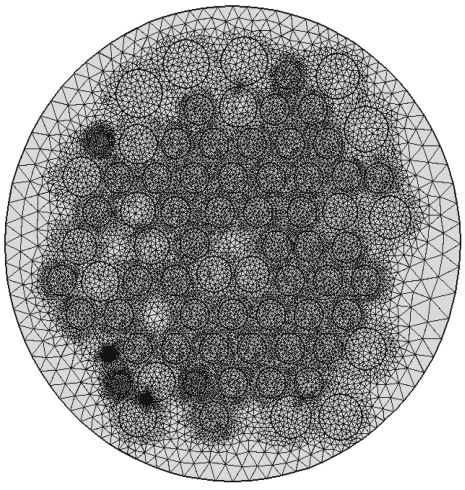


Fig. 2. Irregular microstructure fiber model in which the cross section of fiber is divided into many triangular meshes.

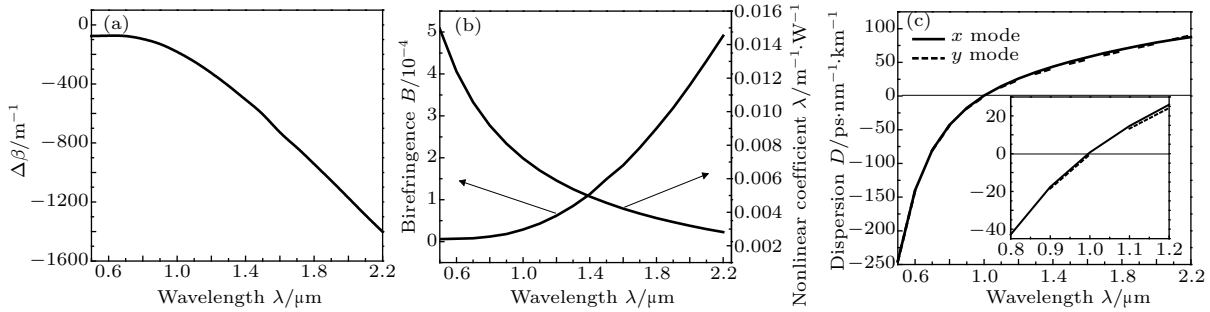


Fig. 3. (a) The propagation constant difference $\Delta\beta$ of the orthogonal polarization-mode versus wavelength. (b) The nonlinear coefficient and birefringence degree versus wavelength. (c) Dispersions of the two orthogonally polarized modes versus wavelength. The zoom view is also shown in panel (c).

3. Experimental results and analysis

The experimental principle is shown in Fig. 4. A 60-cm long fiber is used in the experiment. The pumping source is a Mira900 Ti sapphire laser whose average output power is 0.6 W, pulse width is 120 fs, pulse type is hyperbolic secant, repetition frequency is 76 MHz, and the adjustable central wavelength is between 700 nm and 980 nm. The spectrometer is an AvaSpec-2048-USB2 whose measurement wavelength is in the range 200 nm–1100 nm. The other spectrometer is an infrared spectroscopic analyzer, Avaspec-NIR256-NIR-25, whose measurement wavelength is in the range 9002 nm–2500 nm and whose precision can reach 5 nm–10 nm. The nonlinear coefficient of PCF can be expressed as,[12]

$$\gamma = \frac{8\pi^2}{\lambda^3} n_2 b_2 (n_\mathrm{b} - n_\mathrm{eff}),$$

where n_2 is the nonlinear refractive index coefficient. For the quartz optical fiber, usually, $n_2 = 3.0 \times 10^{-20}$ $\mathrm{m}^{-1}\cdot\mathrm{W}^{-1}$, n_b is the refractive index of the fiber matrix material, which can be obtained using the Sellmeier formula,[13] n_eff is the effective refractive index under the fundamental mode. Since the effective refractive index along the fast axis of optical fibers is small, the corresponding nonlinear coefficient is large. In the experiment, the polarization direction of the incident light pulse is controlled by adjusting the angle of the half-wave plate. When the nonlinearity is strongest, that is, the spectral broadening degree is highest, the polarization direction of optical pulses is parallel to the fast axis of the fiber. The optical output power of the incident light is controlled by adjusting the attenuation plate. It can be seen from Fig. 3(c) that the zero-dispersion point of the PCF is nearly at a wavelength of 1 μm. In the experiment, efficient frequency conversion is produced by increasing the wavelength of the incident pulse to make the pulse work in the normal dispersion regime. In contrast, large frequency conversion usually happens in the abnormal dispersion section of fibers, as indicated in previous reports.[14–19] It can be seen from Fig. 5 that when the wavelength of the incident light pulse increases gradually from 778 nm to 818 nm, the strength of the anti-Stokes wave increases rapidly. The intensity of the anti-Stokes wave corresponds to the increasing rate of the long-wave Stokes wave intensity, which can even exceed the intensity of the residual pumping wave. The main reason is that the closer to the zero-dispersion point the wavelength is, the more remarkable the four-wave mixing will be under phase matching between Stokes waves of pumping wave in the long wave band, which leads to the rapid growth in the frequency spectrum composition in the short wave band. Meanwhile, in the long wave band (abnormal dispersion section), there also appears a new frequency spectrum (secondary Stokes wave) which forms a soliton under the joint action of the dispersion and nonlinear effect of SPM. The soliton moves to the long wave direction or even appears in the infrared light range of 1700 nm $\sim$ 2100 nm, and at the same time blue-shift waves are formed in the short wave band. Since the nonlinearity of the short wave band is higher than that of the long wave band (as γ is inversely proportional to λ), the intensity of an anti-Stokes wave in the short wave band is higher than that of a Stokes wave in the long wave band. From another aspect, as the central wavelength of the incident pulse gradually increases and turns closer and closer to the zero-dispersion point, the dispersion becomes larger while the dispersion slope becomes smaller. It can be analyzed from Eqs. (1) and (2) that the phase mismatch $\Delta\delta$ also turn smaller and smaller, leading to a more remarkable four-wave mixing effect under phase matching and a larger band frequency shift, more concentrated energy of the Stokes wave in the long wave band and the anti-Stokes wave in the short wave band, and a higher conversion efficiency.

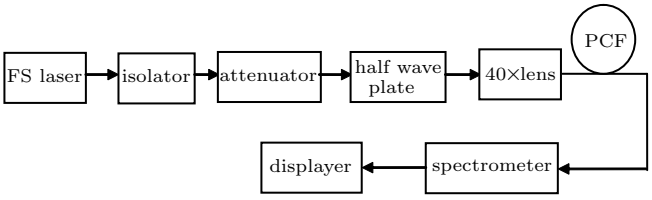


Fig. 4. Experimental setup.

Based on the fiber parameter obtained by simulating the fiber used in the experiment and the pumping pulse parameter used in Fig. 4, figure 6 shows the calculated Stokes waves from Eqs. (1) and (2) and the phase difference $\Delta\delta$ between pumping wave and anti-Stokes wave. The wavelengths which

meet the phase matching $\Delta\delta = 0$ correspond to the positions of anti-Stokes wave and Stokes wave. It can be known from Fig. 5 that as the incident wavelength becomes longer, the positions of anti-Stokes waves and Stokes waves where the phase match condition are located in ranges of about 540 nm–590 nm and 1750 nm–2000 nm, respectively. These are almost the same as the experimental results. The reason why there are no corresponding anti-Stokes waves in the experiment results at the short wavelengths of 470 nm–480 nm may be the loss of spectral energy and the failure to reach the ideal measurement range of the spectrometer.

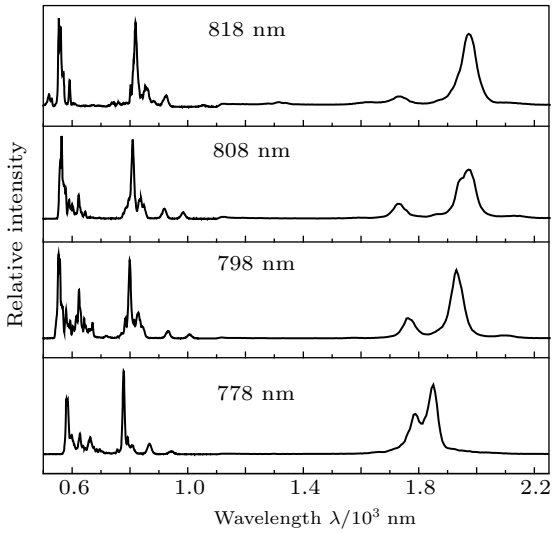


Fig. 5. Output spectra of the microstructure optical fiber with different wavelengths.

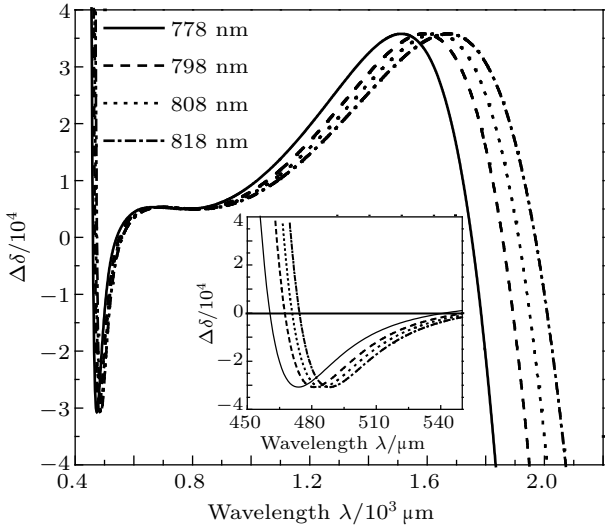


Fig. 6. Curves of phase difference $\Delta\delta$ between the pump pulse and dispersive wave versus wavelength. The inset shows a local zoom view.

When the pumping wavelength is 808 nm and the average powers of the incident pulse are 0.3 W, 0.4 W, and 0.63 W, the spectra are shown in Fig. 7. What is produced on the left side of the pumping wavelength is an anti-Stokes wave, and on the right side there appears a Stokes wave. It can be seen from Fig. 7 that when the power is 0.63 W, an efficient anti-Stokes wave and Stokes wave are produced near 560 nm and 2000 nm respectively. The central pumping wavelength is 808 nm and the zero-dispersion wavelength of the fiber is around 1000 nm, so the pumping is within the normal dispersion regime of the fiber. Since it is relatively close to the zero-dispersion wavelength of the fiber, the second order dispersion β_2 is very small and high-order dispersions all have a large influence on the four-wave mixing. When the pulse laser starts to be coupled into the fiber, it is mainly the SPM that broadens the frequency spectrum. In the broadened frequency spectrum close to the zero-dispersion frequency of microstructure fiber, photons with degenerated frequencies can act as the pumping photons for the four-wave mixing of phase matching. These photons transfer their own energies into the normal dispersion section (< 1000 nm) and abnormal dispersion section (> 1000 nm). XPM makes the frequency spectrum become broader asymmetrically; the Raman scattering, high-order dispersion and self-steepening effect can also cause asymmetrical distribution of the frequency spectrum. As shown in Fig. 7, there is a strong anti-Stokes wave and a Stoke wave near 560 nm and 2000 nm, respectively. When the average power of the pulse increases from 0.3 W to 0.63 W, the energy of the Stokes wave is tripled, and the energy of the anti-Stokes wave increases almost by ten times. The peak powers of anti-Stokes/Stokes waves and the residual signal of pumping waves reach up to 1.12 and 0.67, respectively. Meanwhile, it can be seen from Fig. 7 that with the increase of the incident pulse power, the central wavelengths of the produced Stokes and anti-Stokes waves move closer to long wave and short wave, respectively. The spectrum becomes broader. This is because the higher the power is, the more strongly the nonlinear terms act in the parametric process $2\omega_{\rm P} = \omega_{\rm s} + \omega_{\rm a} + 2\gamma p_0$, and the more frequency spectrum compositions in the four-wave mixing there will appear.[20,21]

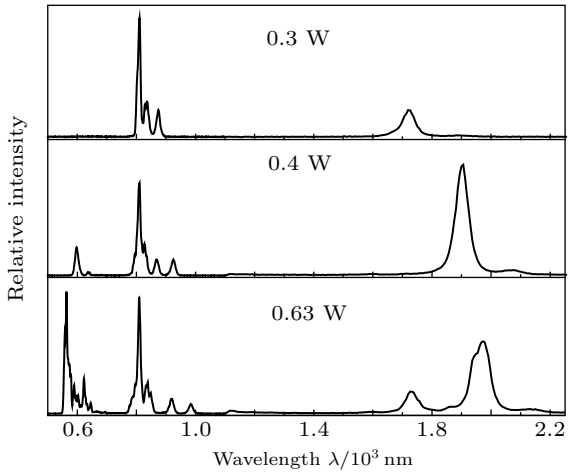


Fig. 7. Output spectra of the microstructure optical fiber with different incident pulse powers.

The difference in the dispersion curve between long and short axes is allowed to be taken as an adjustable dimension in the parametric process of nonlinear optics for the incident polarized light beams with different polarization directions. The experiment obtains Stokes waves and anti-Stokes waves of different central wavelengths by changing the polarization state of the incident pulse. The spectra obtained in the fiber are shown in Fig. 8 when the central wavelength of the pulse output from the femtosecond laser is 798 nm, the average power of input pulse is 0.43 W, and the polarization direction of the input pulse is parallel or perpendicular to the direction of the fast axis. It can be seen that the Stokes wave and anti-Stokes wave are obviously higher when the polarization direction of the input pulse is parallel to the fast axis than when the polarization direction of the input pulse is perpendicular to the fast axis. Despite this, the intensities of both Stokes waves and anti-Stokes exceed those of the residual pumping waves, with conversion efficiency over 60%. Due to the ellipse structure of the fiber core, the dispersion curves of different polarization directions are different; and the central wavelengths of anti-Stokes waves and Stokes waves under phase match shift under the action of femtosecond laser pulses with different polarization directions. In the two orthogonal polarization directions, peak values of anti-Stokes waves appear at the wavelengths of 619 nm and 557 nm with a shift of 63 nm, and peak values of Stokes waves occur at the wavelengths of 1740 nm and 1900 nm, with a shift of 160 nm. It can be seen from Fig. 8 that there are multiple peaks at the signal points of anti-Stokes. This is mainly because the anisotropic core structure enables the models of different polarization and dispersion characteristics to interact with each other, causing the model of an anti-Stokes wave to be replaced by a higher order mode, resulting in the fact that at the output of the fiber, the new frequency signals represent a new peak in the figure. Since the Raman scattering and stimulated Raman scattering in the pulse largely influence the phase matching of the fiber, in the normal dispersion region of the fiber, there will be a cascade Raman effect, four wave mixing, XPM, and high-order nonlinear effect, all of which are factors causing the irregularities of the frequency spectrum.[22–24]

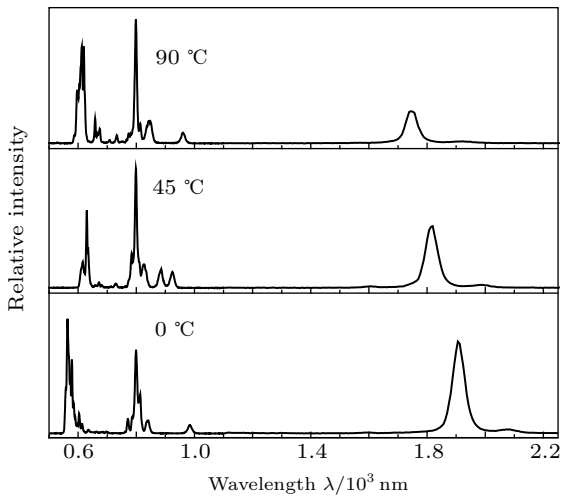


Fig. 8. Output spectra of the microstructure optical fiber with different angles.

4. Conclusion

In this paper, we report a femtosecond laser pulse transmission experiment with home-made cladding ventage disordered high nonlinear birefringent microstructure fibers and study the conversion of wavelengths produced by the four-wave mixing effect in the fiber under different central wavelengths, powers, and polarization directions of the femtosecond laser pulse. The influences of the input laser pulse wavelength, input power and polarization directions on the central wavelength, intensity, and frequency conversion efficiency of anti-Stokes and Stokes waves produced by the fibers are analyzed. It is found that as the incident pulse gradually gets close to the zero-dispersion point, the average pulse power and the angle between the polarization direction and the fast axis of the fiber increase less, the anti-Stokes effect is gradually enhanced, and the conversion efficiency also gradually increases. When the pulse polarization direction is parallel (perpendicular) to the fast axis of the fiber, the central wavelength of the anti-Stokes wave (Stokes wave) in the fiber has a shift of 63 nm (160 nm). The new feature of this microstructure fiber expands the nonlinear effect of an ultrashort laser pulse, providing a new method of solving the problem of phase-matching in nonlinear optics. The microstructure fibers can act as efficient frequency converters for ultrashort pulses and can be used in WDM wavelength conversion technology. The findings in this paper provide theoretical support for wavelength-adjustable broadband mode locking fiber laser seed source technology.

Acknowledgment

The authors are grateful to professor Li Shu-Guang from the Faculty of Science, Yanshan University for his instructive guidance and revision on this paper.

References

[1] Liu X M, Zhou X Q and Lu C 2005 *Phys. Rev. A* **72** 013811
[2] Hu M L and Wang Q Y 2004 *Acta Phys. Sin.* **53** 4243 (in Chinese)
[3] Liu X M 2008 *Phys. Rev. A* **77** 043818
[4] Liu W H and Song X Z 2008 *Acta Phys. Sin.* **57** 917 (in Chinese)
[5] Yu Y Q, Ruan S C, Zeng J C 2005 *Acta Photon. Sin.* **34** 1294 (in Chinese)
[6] Li S G, Ji Y L and Zhou G Y 2004 *Acta Phys. Sin.* **53** 478 (in Chinese)
[7] Chen Y Z, Li Y Z and Qu G 2006 *Acta Phys. Sin.* **55** 717 (in Chinese)
[8] Zhang X J, Li H P and Liao J K 2010 *Optics & Optoelectronic Technology* **8** 4
[9] Shen X W, Yu C X and Sang X Z 2012 *Acta Phys. Sin.* **61** 044203 (in Chinese)
[10] Guo C Y, Sun X Y and Li A P 2009 *Study Opt. Commun.* **4** 154
[11] Sun X W, Wang Q Y and Hu M L 2007 *Acta Photon. Sin.* **36** 1 (in Chinese)

[12] Qiu J C, Liu H K and Tian X X 2007 *Journal of China West Normal University (Natural Sciences)* **28** 4 (in Chinese)
[13] Saitoh K, Koshiba M and Mortensen N A 2006 *New J. Phys.* **8** 207
[14] Yu L R, Yin J and Wan H 2010 *Acta Phys. Sin.* **59** 5406 (in Chinese)
[15] Chen B 2008 *Policy & Management* **23** 63
[16] Sun T T, Wang Z and Li C Q 2009 *Chin. J. Lasers* **36** 154
[17] Stark S P, Biancalana F and Podlipensky A 2011 *Phys. Rev. A* **83** 23808
[18] Sørensen S T, Judge A, Joly N Y and Russel P S 2010 *J. Opt. Soc. Am. B* **27** 592
[19] Cascante-Vindas J, Diez A, Cruz J L and Anders M V 2010 *Opt. Express* **18** 14535
[20] Cascante-Vindas J, Torres-Peiro S, Diez A and Andres M V 2010 *Appl. Phys. B: Laers* **98** 371
[21] Labruyère A, Leproux P, Couderc V, Tombelaine V, Kobelke J, Schuster K, Bartelt H, Hilaire S, Hilaire S, Huss G and Melin G 2010 *IEEE Photon. Technol. Lett.* **22** 1259
[22] Hu M L, Li Y F, Chai L, Xing Q, Doronina L V and Ivanov A A 2008 *Opt. Express* **16** 11176
[23] Hao Z J, Zhao C J, Wen J G, Wen S C and Fan D Y 2011 *Acta Opt. Sin.* **31** 10060031 (in Chinese)
[24] Fedotov A B, Voronin A A, Fedotov I V, Ivanov A A and Zhenltikov A M 2009 *Opt. Lett.* **34** 851